Advanced Quantum Technologies

ADVANCED QUANTUM TECHNOLOGIES
www.advquantumtech.com

RESEARCH ARTICLE OPEN ACCESS

Enhancement of Coherence Times of Individual Shallow NV Center due to Ozone Treatment

Jéssica Fernanda da Silva Barbosa[1] | Angelika Kaiser[1] | Alma Beatrice Sergi[1] | Allegra de Gleria Clark[2] | Johannes Lang[2] | Christoph Findler[2] | Christian Osterkamp[2] | Jakob Buchheim[1] | Markus Mohr[1]

[1]German Aerospace Center (DLR), Institute of Quantum Technologies, Ulm, Germany | [2]Diatope GmbH, Ummendorf, Germany

Correspondence: Jéssica Fernanda da Silva Barbosa (jessica.dasilvabarbosa@dlr.de)

Received: 7 November 2025 | **Revised:** 26 March 2026 | **Accepted:** 6 April 2026

Keywords: ozone surface treatment | shallow NV center | spin coherence time

ABSTRACT

Shallow nitrogen vacancy (NV) centers with long coherence times are promising candidates for applications in areas such as quantum computing and quantum sensing. However, as the NVs are only a few nanometers below the diamond's surface, it is a challenge to remove the different decoherence sources related to the surface, e.g., charge fluctuations and magnetic impurities. Here, the effect of ozone treatment on the chemical composition of diamond surfaces was correlated with its impact on the spin properties of the same individual shallow NV (depth < 20 nm) by comparing its coherence times, Ramsey (T_2^*) and Hahn Echo (T_2), before and after the treatment. X-ray photoelectron spectroscopy (XPS) shows a reduction in sp^2 bonds, and it was reported that an enhancement of the coherence times up to a factor of 3. Additionally, we investigate the effects of Ozone treatment on random single NVs engineered to have a depth of ∼30 nm, where an enhancement up to a factor of 10 on T_2^* and up to a factor of 3 on T_2 have been observed.

1 | Introduction

Nitrogen vacancy (NV) centers in diamond [1] are color centers well known as robust quantum systems. They have been widely studied in the last decades due to their outstanding properties, such as the Optically Detected Magnetic Resonance (ODMR) associated with long coherence times at room temperature [2, 3]. Quantum computers based on NV centers in diamond were proposed long ago [4] and commercial room temperature quantum computers with four qubits have been achieved recently [5]. Scaling up the number of qubits in a diamond NV based quantum computer is often pursued by making use of dipolar coupling between two or more NV centers [6–9]. If they are created by implantation, shallow NVs are beneficial due to the smaller lateral straggling and the higher probability to place NV centers at distances small enough to achieve strong dipolar coupling. Several approaches for a scalable quantum computer device based on NV centers in diamond indeed make use of shallow negatively charged NV^- centers (< 100 nm distance from the surface) [7–9]. The challenge for shallow NVs is, however, the shorter coherence times, on the order of a few µs [10] due to magnetic and electric noise sources at the surface [11–16] in comparison to deeply implanted ones, which show coherence times exceeding 2 ms [2].

NV centers in diamond are formed by a substitutional nitrogen atom next to a vacancy [17] and can be formed naturally or artificially, e.g., via ion implantation and annealing [18, 19]. They can be found in three different charge states: positive NV^+, zero NV^0 and negative NV^-. NV^0 presents five electrons: three from the carbon dangling bonds and other two from the nitrogen unpaired electrons. It presents spin $S = 1/2$ and photoluminescence (PL) under green illumination, but cannot be manipulated via ODMR. By losing an electron to the environment, NV^0 becomes NV^+,

without electronic spin ($S = 0$) and no measurable PL. On the other hand, by trapping an extra electron from the surroundings, NV^0 turns into NV^- leading to an electron spin triplet that can be initialized and controlled at room temperature by ODMR. In the following, if it is not specified, it will be used the notation NV to refer to NV^-.

Suppression of the creation of multi-vacancy complex defects during CVD growth on n-type of diamond has been reported [20] as an approach to enhance NVs coherence times, as well as a precise control of surface termination. This work focus on the latest. While a hydrogen-terminated diamond [21], which is usually present after diamond growth by chemical vapor deposition, has a low surface defect density [22], its absence is often desired, since it gives rise to a sub-surface hole accumulation layer (negative electron affinity) that can convert the shallow NV^- into NV° centers [23]. Another important noise source is sp^2-bonded carbon on the surface [22] which prevent the stability of NV^- within a certain depth from the surface. Hence, a termination that leads to a surface upward band bending is desired for charge stabilization and the most common method is the oxygenation of the surface [24–33].

A large variety of processes are known to lead to an oxygen termination of the diamond surface, such as oxidation in acids [34, 35], by ozone [27, 28, 36, 37], in oxygen atmosphere [29], as well as in oxygen plasma [29, 38] and oxygen annealing [39]. Oxygen can be attached to the diamond surface in several configurations, such as in an ether group, in a hydroxyl group, or in a ketone group, and is usually present in all of these three configurations [27, 28]. Different surface oxygen termination procedures lead to different outcomes in terms of electron affinity [40] and NV performance [33].

Ozone treatment is a well stablished treatment [41] that can be produced via different processes as listed in [42]. In the recent years, ozone has been extensively used as surface treatment method for diamond surfaces in order to obtain smooth surfaces [43], in particular nanodiamonds [44–46]. Their behavior on the rabi oscillations' contrast of ensembles of NVs has already been investigated [47]. In this work the effects of standard ozone treatment in the diamond surface are correlated with the spin properties of single shallow NV centers. Characterizing the same individual shallow NVs before and after the ozone treatment leads do the establishment of intrinsic correlation between the shallow NV coherence times and the properties of the diamond surface. This opens a way to surface engendering optimization that could inspire new studies toward NVs on diamond-based quantum technologies.

2 | Samples

In this work we use two commercial diamond substrates from Element Six ($4.0 \times 4.0 mm^2$, 0.50mm thick, 1.1% ^{13}C, substitutional Nitrogen < 5 ppb, Boron < 1 ppb, NV < 0.03 ppb, {100} surface). In order to etch reference markers of 100 nm depth, a bi-layer photolithography lift-off process was used to structure an Aluminum etch mask, which was evaporated onto the diamond. The markers were etched into diamond with a reactive ion etching (RIE) process using an oxygen plasma. The Aluminum etched mask was removed by a H_2SO_4:H_2O_2 mixture and the samples were subsequently cleaned using a triacid solution. Further information can be found in the supporting materials. Using plasma enhanced chemical vapor deposition, a 100 nm thick layer of isotopically purified ^{12}C diamond was grown on top of both samples (Diatope GmbH). Figure 1 shows the sketch of the two samples used in this work. The NV centers of **Sample A** were formed by nitrogen ion implantation of 5×10^8 ions/cm^2 of $^{15}N^+$ with an energy of 5 keV, followed by vacuum annealing at 1373.15 K (1100°C). **Sample B** was implanted with 1×10^{11} ions/cm^2 of $^{15}N^+$ at 5 keV followed by an additional overgrowth of 20 nm of ^{12}C purified diamond, and subsequently annealed in vacuum at 1373.15 K (1100°C) as described in [34]. It was implanted the specific isotope of nitrogen ions, ^{15}N, in order to ensure that the investigated NV centers were formed by implantation rather than naturally. In the following, it will be used the notation N to refer to ^{15}N ions. The expected depth of the NVs in Sample A is around 10–15 nm below the surface and it was simulated in SRIM. Thus, the NV centers on Sample B are expected to be 20 nm deeper (30–35 nm) than in Sample A.

Both samples were treated with ozone in a home-made setup, and they were characterized before and after that treatment. The Experimental details are described in Section 6 of Experimental Methodology.

3 | Results

3.1 | Surface Topography

Both samples have been measured in the AFM after NV creation and before ozone treatment. Figure 2a shows the acquired topographies, $(30 \times 30)\ \mu m^2$ of Sample A (left) and Sample B (right). They were planarized with a second-order polynomial with the open-source software Gwyddion. On top of each scan, the height profile corresponding to the yellow line traced on the topography image perpendicularly to the polishing lines is shown.

The characteristic wavy and inhomogeneous lines derived from mechanical polishing and they are evident in both samples. By extracting height profiles, we estimated the maximum difference between consecutive mountains and valleys, i.e., 2.5 and 1.5 nm for Samples A and B, respectively. RMS roughness calculated in Gwyddion on the full $(30 \times 30)\ \mu m^2$ scans is around 710 pm for sample A and 550 pm for sample B. For comparison, the RMS of the as-received substrates is 1049 pm, and its AFM measurement in shown in Figure S10.

3.2 | Surface Chemistry

Survey spectra of samples A and B after NV centers creation and before surface treatment with ozone are shown in Figure S1a,b. Evaluation of the survey scans for both samples show the presence of carbon (C, 91 at%) and oxygen (O, 8 at%) as the main elemental contributions of the sc diamond surface. The C contribution mainly represents the diamond bulk, while the O contribution is the direct result of diamond surface oxidation due to tri-acid boiling procedure during sample initialization. Sample A shows additional elemental residue of copper (Cu, <

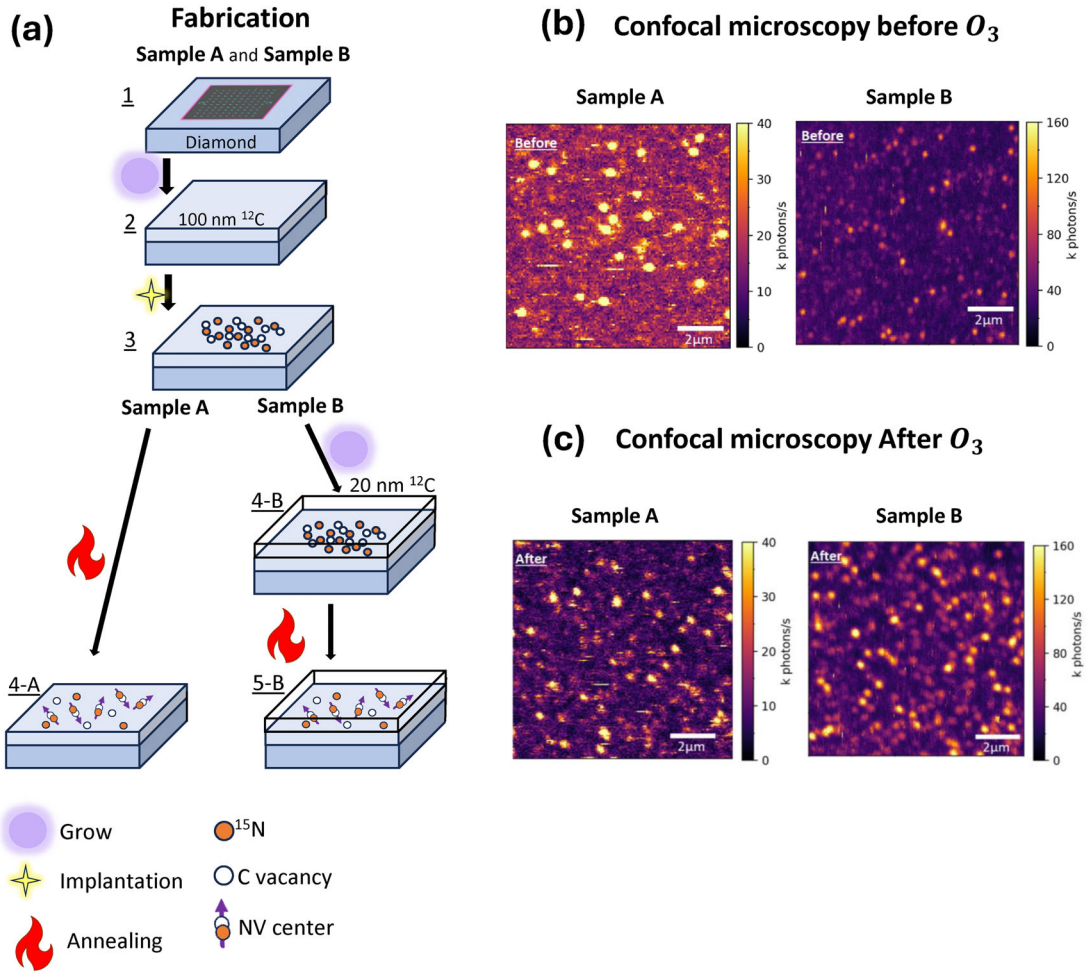

FIGURE 1 | Sample fabrication and characterization. (a) fabrication process of the two investigated samples: 1) creation of etched marks using Al masking and RIE 2) growth of a 100 nm isotopically purified ^{12}C diamond layer 3) ^{15}N implantation. 4-A) sample A is annealed after ion implantation 4-B) sample B is overgrown with a 20nm of ^{12}C diamond layer and 5-B) annealed. (b) – (c) Spin characterization: confocal microscope image of both samples before and after Ozone treatment, respectively.

1 at%) and lead (Pb, < 1 at%) on the diamond surface (Figure S1a insets). Traces of Cu and Pb for A are a result of soldering the wire antenna. A display and direct comparison of the C 1s and O 1s high-resolution scans of both samples (Figure 2b left) indicate no noteworthy difference, hence the trace contaminations do not seem to change the results of diamond surface chemistry fundamentally. However, the presence of Cu and Pb still suggests less contamination prone methods for microwave antenna integration for the spin-characterization. The following evaluation of C 1s and O 1s high-resolution scans applies to both samples. O 1s detail scan spectra (Figures S2 and S3) show a singular broad contribution at 531.4 eV with a FWHM (full-with-half-max) of 2.2 eV, hinting toward a multitude of oxygen-related functional groups on the diamond surface. The deconvolution of the C 1s detail scan spectra is shown in Figure 2b. The main signal contribution originates from sp^3C (284.8 eV) representing sc diamond bulk. The peak component at lower BE indicates non-diamond sp^2C phase (283.6 eV) representing surface defects of the sc diamond lattice. The chemical shift of – 1.2 eV is in agreement with most reported assignments regarding the difference between sp^3C and sp^2C [48, 49]. Some works relate the formation of sp^2C phase to initial oxidation processes, like the tri-acid treatment itself [27]. It can be further interpreted as precursor site for the formation of graphite on diamond [50]. The correct assignment of sp^2C in relation to sp^3C requires caution, due to suspected charging effects, caused by disconnected electron pathways between conducting defects and insolating bulk diamond [48]. Moreover, an increment of FWHM of the C 1s due to a contribution at lower BE could also originate from further complex carbon defects [48]. Deconvolution of peak components toward higher BE show oxygen related functional groups, namely C—O (285.6 eV), C═O (286.6 eV), and C—O═C (287.6 eV) representing the surface oxidation mentioned above. It is assumed that sp^2C carbon is faster oxygenated [27], and early-stages of oxidation are directly linked to sp^2C. Following the assumption of oxidized surface, non-diamond carbon below, and sp^3C diamond as the bulk [27], it is assigned the chemical shifts of oxygen-related functional groups to + 2, + 3, and + 4 eV with respect to sp^2C. This is in good agreement with general fitting parameters of oxygenated graphitic/non-diamond carbon material [51]. A comparison of bulk-sensitive and surface-sensitive data in Figure 2b for sample A (middle) and sample B (right) confirms that oxygen-related contributions and sp^2C contribution are overlayers on top of the sp^3C sc bulk diamond substrate, due to an increased relative intensity in the surface-sensitive data. Applying equation A to the bulk-sensitive C 1s data, shows that the diamond surface is

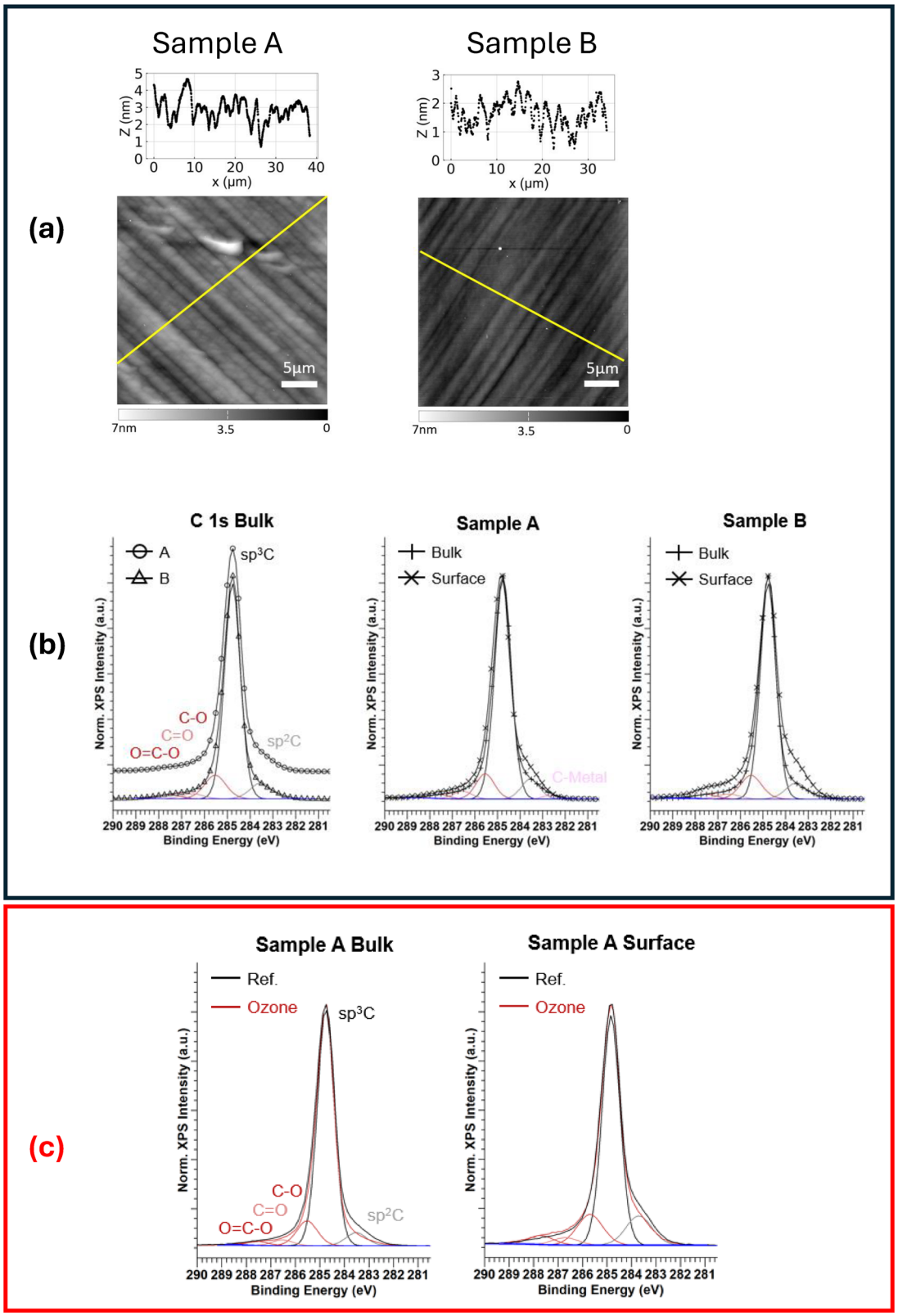

FIGURE 2 | Surface characterization. (a) AFM profile: scan 30μm × 30μm for Samples A (left) and B (right). On top of each image is shown the height profile. (b) Overview of C 1s high-resolution scans of Samples A and B before surface treatment with ozone. Left: direct comparison of C 1s peak shapes and respective contributions. Center and right: Angle resolved XPS of Sample A and B, respectively, shows that oxygen-related contributions and sp^2C contribution represent overlayers on the defect-free sp^3C sc diamond substrate and hence are native to the surface treatment. (c) C 1s high-resolution scans of Sample A after surface treatment with ozone including. Left: bulk-sensitive data; Right: surface-sensitive data. For better display, ozone-treated data (red) is displayed alongside ref. data to highlight that ozone treatment drastically reduces the sp^2C contributions.

dominated by an oxidized sp^2C diamond overlayer of 0.5 nm thickness, i.e., ~5 sp^3C diamond monolayers.

Since the surface of both samples is chemically equivalent, as shown by Figure 2b, was performed only in Sample A to investigate the effect of the ozone on diamond surface. Figure S1c shows the survey scan of sample A after consecutive tri-acid boiling and ozone treatment. Aside of the expected contributions (C and O) no additional elemental traces can be found. Previous Cu and Pb residue were successfully removed after tri-acid boiling. In comparison to the untreated surface, the general chemical composition of the sample surface remains unchanged. However, after ozone treatment the contribution of the sp^2C in the bulk-sensitive high-resolution C 1s scan is drastically decreased, which is evident by a reduced intensity of said contribution. Applying equation A to the bulk-sensitive scan shows a reduction of the oxidized sp^2C diamond overlayer down to 0.1 nm, which is equivalent to only 1 – 2 monolayers of sp^3C diamond. This calculated overlayer thickness now exceeds the application limit of equation A. For the surface-sensitive scans, the reduction of the sp^2C overlayer is visible, however less pronounced. Here, the information depth of the surface-sensitive measurement matches the height profile of the surface topology. A display of raw signal intensity of sample A (Figure S2) indicates a strong impact of shadowing effects, which is visible during repeated surface-sensitive measurements. Hence, no quantitative information is drawn from comparison of surface-sensitive measurements.

Ozone treatment causes a drastic reduction of previously defective sp^2C diamond and enhances the presence of defect-free sp^3C diamond. This is also evident in a slightly reduced FWHM of sp^3C, which further hints at defect removal. We suggest that ozone forms simplest oxides of carbon, which then desorb from the diamond surface. The ozone treatment does not heavily alter the oxidation layer (O, 8 at%) of the initially oxidized diamond surface. This supports findings, which suggest a lower oxidation ability of ozone treatment in comparison to more conventional oxidation methods, e.g., tri-acid boiling or O_2 plasma [28]. The general abundance of the C—O (285.6 eV), C═O (286.6 eV), and C—O═C (287.6 eV) contributions remain. The relative abundance of C—O═C (287.6 eV) related bonds appear to be slightly elevated after the ozone treatment. This change to the oxygen-related termination which is also evident in high-resolution scan of the O 1s region (Figure S4). Here, the overall peak shape slightly changes, which hints at a redistribution of the possible oxygen-related bonds.

In addition, the role of ozone was investigated on a heteroepitaxial CVD-diamond (test diamond). Chemical analysis was performed before and after ozone treatment, leading to similar results (Figure S5). This further solidifies our findings to the beneficial impact of ozone on oxidized sp^2C diamond surface.

3.3 | Spin Characterization

The confocal image of both samples before and after Ozone treatment are shown on Figure 1b,c. In both samples the density of bright spots increased after ozone treatment. Table 1 summarizes the fabrication yield of NVs (implanted N/formed NVs) for both samples before and after the ozone treatment.

TABLE 1 | Yield. The effect of ozone treatment in the NV's yield formation for both samples.

	Yield before O3 [%]	Yield After O3 [%]
Sample A	2.7	4.1
Sample B	0.00093	0.03

After ozone treatment, the yield has enhanced by a factor of 1.5 and 32 for Samples A and B, respectively. In addition, the confocal microscope image presents a reduction of the background PL from diamond surface after the treatment.

As to the spin properties, in order to distinguish the influence of the surface treatment from other bulk crystal-related influences (strain, coupling to other defects, etc.), for Sample A we compared the performance on the same 6 NVs before and after the treatment.

The summary of their coherence time as a function of the depth are shown in Figure 3a,b, Ramsey and Echo respectively. As to the Ramsey (T_2^*), one can see that ozone treatment has a beneficial effect for all NVs deeper than 8 nm. The enhancement factor, however, differs from NV to NV been from 0.7 ± 0.2 to 3.2 ± 0.7. In the best case, T_2^* was 2.1 μs and becomes 6.8 μs. Before ozone treatment, Echo (T_2) and Ramsey (T_2^*) times were comparable but after the treatment the ratio T_2/T_2^* enhanced for all NVs from a factor of 1.4 ± 0.2 to 4.1 ± 0.4. As to ODMR and Rabi, there was no contrast enhancement as one can see in Figure S7.

On Sample B, the large increase of bright fluorescence spots after the ozone treatment has prevented finding exactly the same NV for spin characterization after the treatment. Thus, for this sample we measured 2 different sets of NV centers at the same region. Figure 3c,d shows the measured values of T_2^* and T_2, respectively. The NVs measured before (after) ozone was labeled with Romans (Greek) letters.

Before ozone treatment T_2^* and T_2 were shorter than: $T_2^* < 2.5$μs and $T_2 < 200$μs, respectively. Those values are in the same order of magnitude of what is reported in literature [34]. On the other hand, after ozone treatment the coherence times were more distributed and although coherence times similar to NV set 1 are founded, there are several NVs presenting much longer coherence times: up to 14.5 ± 2.7 μs for T_2^* and 400 ± 49 μs for T_2. Moreover, in the NVs measured after ozone, the contrast of both ODMR and Rabi have enhanced by a factor 2.

4 | Discussion

4.1 | Surface Topography and Spin Properties

The coherence times enhancement factors vary from NV to NV, even for those at the same depth. This can be attributed to electric and magnetic fluctuations [52], surface roughness noise [53] and other defects in the crystal lattice close to the specific NVs inside the diamond layer. Thus, the impurity density seen by the NVs is not homogeneous and therefore the effect of the global treatment

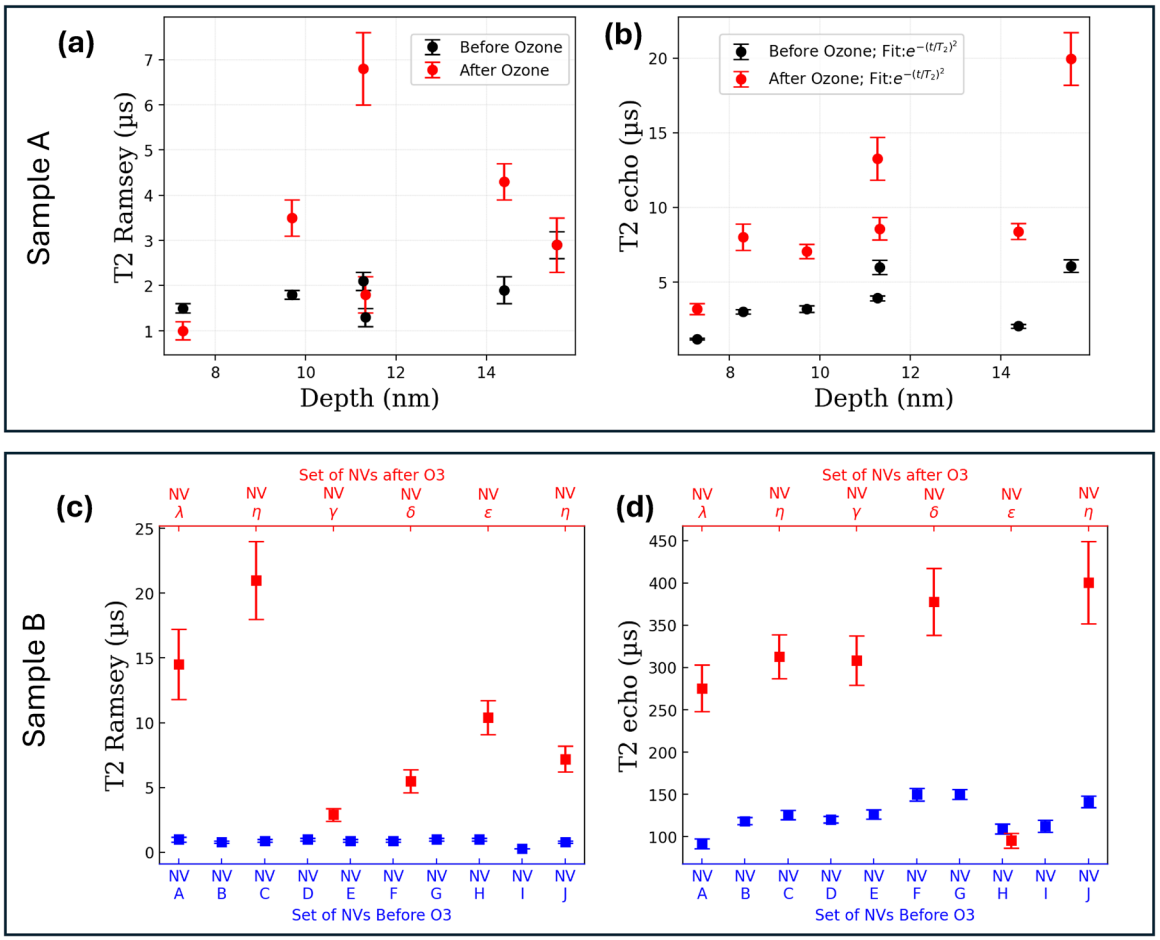

FIGURE 3 | Spin properties. (a)[c] and (b)[d] show the measurements of T_2^* and T_2 echo of Sample A[B]. The black [blue] points refer to NVs measured before ozone treatment while red points refer to after O3 treatment. In Sample A, the same NV was measured again after ozone treatment while in Sample B two different sets of NVs were investigated.

is pondered by the initial concentration of defects at NV close vicinity.

Moreover, from the RMS values and the observation of the polishing lines, Figure 2a, one can conclude that the second overgrowth of 20 nm on sample B leads to a smoother surface with respect to Sample A, i.e., less charge density fluctuation and, therefore, ozone treatment is more efficient in reducing electrically noise and the scattering photons from the surface of Sample B.

4.2 | Surface Spectroscopy and Spin Properties

In accordance with previous work [28, 32, 54, 55], the present ozone treatment also leads to surface oxidation as well as a significant reduction of sp^2 C bounds, as shown by XPS data. This reduction mainly occurs at the first two Carbon monolayers and induces a change in surface band bending [22]. These changes in the surface affect several NV spin properties such as conversion yield, PL background, PL contrast and its coherence times. The effects of the ozone as well as other treatments that leads to oxygen termination are highly dependent of the sample roughness [43, 39] and the eventual other surface pre-treatments [56] as detailed in [44] where ozone is used to treat nanodiamond and on [39] where the oxygen termination depends on the process used as well as the final sample roughness. This is also suitable for the samples used in this work: the pre-treatment of diamond surface for NV creation provided different efficiencies of the ozone treatment.

4.2.1 | Charge Stabilization and Yield

The enhancement of NV formation yield shown in the confocal microscope images arises from NV charge state stabilization due to ozone treatment. It has been detailed reported in [22] that Fermi-level pinning and NV charge state properties [23] at diamond surfaces are dominated by primal sp^2 defects. Also in [22], it is shown that the band-bending depletion depth depends on the concentration of dopants (in the case, N ions). This is also valid after tri-acid cleaning which not only oxygenated but also creates sp^2 defects on the surface, as detailed investigated by Near-edge x-ray absorption fine structure (NEXAFS) in [39].

For concentrations similar to the one of Sample B [A], the surface coverage with sp^2 will induce a Fermi-level pinning below the NV^-/NV^0 transition level, leading to NV instability within up to 250 nm [40] from the surface. Surface treatments, such as oxygen plasma treatment [25], oxygen atmosphere annealing [26] and the

ozone treatment investigated in the present work, that reduces sp^2 defect density which lead improvement of NV^- charge state stabilities.

Therefore, the difference in the efficiency of the ozone treatment, with respect to the yield, between Sample A and B can be attributed to the difference in their concentration of implanted N ions (2 orders of magnitude).

Our hypothesis, however, is only based on the photoluminescence (PL) intensity of the defects (NV^- is brighter than NV^0). Since also other bright defects can be formed during NV center implantation, such as P1, vacancies agglomerate and also H clusters [57], further investigation must be done in order to validate this theory e.g. measuring only NV^-, before and after Ozone treatment, using a 650 nm long pass filter (NV^- is the major emitter for wavelength larger than 650 nm) associated with excitation laser smaller than the Zero Phonon Line (ZPL) of NV^0 (λ<575) to avoid NV^0 excitation [58].

4.2.2 | PL Background and Contrast

The PL background and contrast are correlated figures of merit for any sort of applications of NV-based quantum technologies. They are directly associated with quantum sensor sensitivity and efficiency as well as the qubit fidelity. Optimization of the signal-to-noise requires low PL background and high contrast.

The ozone treatment also reduced the PL background in the confocal image on both samples, as shown on Figure 1b. Moreover, sample B has provided brighter NVs after ozone treatment.

With respect to the Rabi and ODMR contrast, the samples present distinct behavior: Sample A, where the same NVs was investigated before and after, does not present any enhancement in the Rabi contrast, associated with charge state stabilization. Instead, it presents an enhancement of the T2 and T2* without changes in the contrast. This indicated that the NVs were already charge stable and the ozone eliminated local noise source, providing better distribution of the previous termination or smoothly etched the surface.

For Sample B, the NVs after the treatment do present a systematic enhancement in contrast in both ODMR and Rabi of a factor of 50 per cent. This effect has already been reported in [47] and is due to NV charge state stabilization induced by ozone treatment.

4.2.3 | Coherence Times

Due to the strong reduction of sp^2 C bonds and surface oxidation, the ozone treatment was also beneficial for NV spin coherence times due to a global reduction of the electrical noise in the diamond surface [12, 52]. For the only NV at 8 nm, however, T_2^* turned out shorted after the treatment (in both cases smaller than 2μs) while T_2 enhances. This indicates that locally this shallow NV is coupling with some unknown incoherence sources (e.g. crystalline defects) that dominate its dynamics.

Before ozone treatment, Sample A presents T_2 in the same order of magnitude of T_2^* and although both times enhanced after the treatment. That indicates that the dominant source of decoherence is not effectively decoupled via Hahn Echo sequence i.e., despite the reduction of the sp^2 bounds, the main source of noise remains non-magnetic. The effect of the ozone on smoothing the diamond surface [43] endorses the hypothesis that the enhancement of T_2^* and T_2 in Sample A could be correlated with local remotion of charge density as well as reduction of incoherent photon scattering [53]

On the other hand, Sample B, even before ozone treatment, presented T_2 two orders of magnitude longer than T_2^*, in agreement with the expected value reported in ref [34] for a NV implanted at 5 keV and 20 nm of ^{12}C overgrow. After the ozone treatment T_2^* enhanced by one order of magnitude up to 14.5 μs, and T_2 enhanced by a factor 3. As comparison, T_2 = 2.4μs has been reported for hydrogen-terminated, 15 nm deep NV coated with h-BN [59]. This is evidence that this sample presented both sources of noise but after the treatment the magnetic noise was the dominant.

The effect of ozone combined with Sample B that was undergoing the indirect overgrowth process has been proved very beneficial because on one hand, the overgrowth layer prevents several noise sources from the surface to interact with the spin. On the other hand, the effect of the oxygen termination, that can be seen up to 100 nm from the surface [22], can still affect the spins below this overgrown diamond layer. Moreover, it can compensate the decoherence arising from the high concentration of implanted N ions and the nuclear spin bath of the nitrogen-related defects (substitutional, interstitials, etc.).

5 | Conclusions

We presented the effect of ozone treatment on the top 10 nm diamond surface on oxidation efficiency and reconstruction sp^2C defect bonds into sp^3C. This surface treatment has a direct impact on shallow NV centers spin properties by enhancing its formation yield, contrast, T_2^* and T_2. It is mainly responsible for a reduction of the electric noise. By measuring the same shallow NV before and after, we verify that NV centers response to ozone treatment is not homogeneous but strongly dependent on the spatial density of decoherence source, e.g., crystalline defects in the isotopically purified diamond layer.

Combining Ozone treatment with 20nm of isotopically purified ^{12}C diamond layer, the enhancement of spin properties is even higher: 160% in contrast and T_2^* up to 20 ± 4μs and T_2 up to 400 ± 49 μs for shallow NVs at 30–35nm depth. This is a promising result that helps to enhance the NV performance of quantum computing chips, as well as in quantum sensors based on shallow NVs.

6 | Experimental Methodology

6.1 | Spin Characterization

The created NVs were characterized before and after ozone treatment in a homemade confocal microscope. We used an oil objective PLFLN 100X from Evident Corporation and a frequency

doubled Nd:YAG laser emitting at 532 nm. The sample was mounted on a PCB with a coplanar wave guide, and a soldered wire was used as an antenna to perform ODMR, Rabi, Ramsey and Hahn Echo. The measurements were obtained at an external magnetic field of 47 mT to optimize the PL contrast due to nuclear spin polarization [60]. The microwave pulse sequences were generated by an Arbitrary Waveform Generator (AWG) from Keysight Technologies and the NV depth was obtained by XY8 measurements [61] using the Honeywell Fluka immersion oil (5×10^{28} protons/m^3). Common-mode noise was removed from Ramsey and Hahn Echo measurements using an alternating phase of the last pulse. On Sample A the same 6 NVs were measured before and after the treatment. On Sample B, a set of 10 and another set of 6 different NVs were characterized before and after the treatment, respectively. T_2^* was fitted using a sine exponential decay while T_2 was fitted with the equation:

$$PL = Ae^{-(t/T_2)^p}$$

where PL is the photoluminescence (number of detected photons per second – Normalized), A is the signal amplitude (the contrast), t is experimental variable time, T_2 is the Hahn Echo decoherence time and p is an exponent variable parameter whose value depends on the type and the concentration of the noise [62]. In this work, the values of T_2 were the same, within the error, for either varying p during the fitting or fixing it as p = 2, as shown in (Figure S9). Fixing p = 2, however, provided more precise and accurate fitting, with the minimal values and error for T_2. Moreover, fixing p = 2 is also reasonable for physical reasons since it is characteristic for single NV whose T_2 is limited by spin-bath noise [63, 64] which arises from implanted nitrogen that didn't become NVs for both Sample A and B.

6.2 | Surface Topography

After the first spin-characterization measurements, the surface roughness was measured using a commercial Veeco Dimension 3100 AFM in tapping mode with PPP-NCHR cantilevers from NANOSENSORS. The resulting topographies were then treated and analyzed with the software Gwyddion.

6.3 | Surface Chemistry

XPS measurements were performed before and after ozone treatment on a commercial PHI 5800 X-ray photoelectron spectrometer from Physical Electronics. Excitation spot size was 2.0 × 0.6 mm^2. The excitation source was a monochromatic Al Kα. For machine maintenance and machine setup, the binding energy (BE) scale was initially calibrated with copper (Cu). In total three samples were investigated with XPS, homoepitaxial CVD-grown diamond (sample A, sample B) and heteroepitaxial CVD-diamond (test sample). All samples were insulating solid state materials. Hence, peak positions of interest were determined with respect to the C 1s sp^{3}C contribution, which was set to 284.8 eV binding energy (BE) and represents the defect-free single-crystalline (sc) diamond bulk of said samples. This binding energy calibration was performed with the inbuild charge neutralization system, which controlled expected inhomogeneous charging issues on diamond surface. For measurement calibration on each sample, the intensity of C 1s was maximized, and FWHM of C 1s was minimized. Charge control did not change relative peak positions of core level contributions or relative chemical shifts. Measurements were recorded at $\theta_1 = 45°$, marked as "bulk", and at $\theta_2 = 70°$, marked as "surface". They represent the top ~7 nm and ~3 nm of the sc diamond surface, respectively. Overlayer thickness d was calculated from bulk-sensitive C 1s high-resolution scans following [65].

$$\mathrm{d} = \lambda \mathrm{C\ 1s} * \cos(\theta) * (\mathrm{IC\ 1s\ overlayer/I\ C\ 1s\ substrate}), \quad (A)$$

where $\lambda_{\mathrm{C\ 1s}} = 2.7$ [66] is the C 1s electron mean free path in the overlayer, θ is the photoelectron emission angle, $I_{\mathrm{C\ 1s\ overlayer}}$ and $I_{\mathrm{C\ 1s\ substrate}}$ are the integrated intensities from overlayer and substrate core-level contributions, respectively. Diamond samples were installed on sample trays from stainless steel and fixated with copper clamps. Evaluation was performed by using CasaXPS.

6.4 | Ozone Treatment

The samples were treated in a home-made apparatus using UV exposure. Briefly, ozone was produced by a constant flow of 40 ml/min oxygen (99.999%) exposed to the light of an exterior Xenon XBO 75 arch lamp for 60 min. The total volume of the sample chamber was 12 ml. The generated ozone concentration during UV exposure was measured with ozone test stripes and resulted in at least a concentration of 150 µg/m^3.

Acknowledgements

We appreciate the support from Ulm Center for Nanotechnology and Quantum Material. We thank the Core Facility Elemental, Molecular, and Materials Analysis at University Ulm for XPS measurements. We thank Alberto Pasquarelli for his support with laser lithography. StarQ was made possible by the DLR Quantum Computing Initiative and the Federal Ministry for Research, Technology, and Space (qci.dlr.de/projects/starq).

Open access funding enabled and organized by Projekt DEAL.

Conflicts of Interest

The authors declare no conflicts of interest.

Data Availability Statement

The data that support the findings of this study are available from the corresponding author upon reasonable request.

References

1. M. W. Doherty, N. B. Manson, P. Delaney, F. Jelezko, J. Wrachtrup, and L. C. Hollenberg, "The Nitrogen-Vacancy Colour Centre in Diamond," *Physics Reports* 528, no. 1 (2013): 1–45, https://doi.org/10.1016/j.physrep.2013.02.001.

2. E. D. Herbschleb, H. Kato, Y. Maruyama, et al., "Ultra-Long Coherence Times amongst Room-Temperature Solid-State Spins," *Nature Communications* 10, no. 1 (2019): 3766, https://doi.org/10.1038/s41467-019-11776-8.

3. G. Balasubramanian, P. Neumann, D. Twitchen, et al., "Ultralong Spin Coherence Time in Isotopically Engineered Diamond," *Nature Materials* 8, no. 5 (2009): 383–387, https://doi.org/10.1038/nmat2420.

4. T. D. Ladd, F. Jelezko, R. Laflamme, Y. Nakamura, C. Monroe, and J. L. O'Brien, "Quantum Computers," *Nature* 464, no. 7285 (2010): 45–53, https://doi.org/10.1038/nature08812.

5. D. L. R. eV., All tests passed: DLR QCI accepts 4-qubit demonstrators SQ-RT and XQ1i, last modified (June 27 2025), https://qci.dlr.de/en/all-tests-passed-dlr-qci-accepts-4-qubit-demonstrators-sq-rt-and-xq1i/.

6. P. Neumann, R. Kolesov, B. Naydenov, et al., "Quantum Register Based on Coupled Electron Spins in a Room-Temperature Solid," *Nature Physics* 6, no. 4 (2010): 249–253, https://doi.org/10.1038/nphys1536.

7. C. Findler, J. Lang, and C. Osterkamp, "Diamantelement und Verfahren zur Herstellung eines Diamantelements," Patent EP 4 491 775 A1, Europäisches Patentamt, 2025, https://patentimages.storage.googleapis.com/32/5f/b8/2baf2131e096b1/EP4491775A1.pdf.

8. B. Burchard, "Vorrichtung mit Quantenbus für Einen NV-Zentren Basierenden Raumtemperatur Quantencomputer," Patent DE 10 2020 101 784 B3, Deutsches Patent- und Markenamt, (Nov 26, 2020), https://patentimages.storage.googleapis.com/8e/a6/51/22181d9675b5ae/DE102020101784B3.pdf.

9. J. Meijer, M. Grundmann, M. Bähr, A. Rönisch, T. Gutt, and H. Ehm, "Aufbau- und Verbindungstechnik für Eine NV-Zentren Basierende Quantentechnologische Vorrichtung," Patent DE 10 2020 118 617 A1, Deutsches Patent- und Markenamt, 2022 (Feb 2, 2023), https://patentimages.storage.googleapis.com/7b/cd/13/dc702cc038435f/DE102022118617A1.pdf.

10. J. Wang, W. Zhang, J. Zhang, et al., "Coherence Times of Precise Depth Controlled NV Centers in Diamond," *Nanoscale* 8, no. 10 (2016): 5780–5785, https://doi.org/10.1039/c5nr08690f.

11. M. Kim, H. J. Mamin, M. H. Sherwood, K. Ohno, D. D. Awschalom, and D. Rugar, "Decoherence of Near-Surface Nitrogen-Vacancy Centers due to Electric Field Noise," *Physical Review Letters* 115, no. 8 (2015): 87602, https://doi.org/10.1103/PhysRevLett.115.087602.

12. B. A. Myers, A. Das, M. C. Dartiailh, K. Ohno, D. D. Awschalom, and A. C. Bleszynski Jayich, "Probing Surface Noise with Depth-Calibrated Spins in Diamond," *Physical Review Letters* 113, no. 2 (2014): 27602, https://doi.org/10.1103/PhysRevLett.113.027602.

13. B. A. Myers, A. Ariyaratne, and A. C. B. Jayich, "Double-Quantum Spin-Relaxation Limits to Coherence of near-Surface Nitrogen-Vacancy Centers," *Physical Review Letters* 118, no. 19 (2017): 197201, https://doi.org/10.1103/PhysRevLett.118.197201.

14. Y. Romach, C. Müller, T. Unden, et al., "Spectroscopy of Surface-Induced Noise Using Shallow Spins in Diamond," *Physical Review Letters* 114, no. 1 (2015): 17601, https://doi.org/10.1103/PhysRevLett.114.017601.

15. E. Janitz, K. Herb, L. A. Völker, W. S. Huxter, C. L. Degen, and J. M. Abendroth, "Diamond Surface Engineering for Molecular Sensing with Nitrogen—Vacancy Centers," *Journal of Materials Chemistry C* 10, no. 37 (2022): 13533–13569, https://doi.org/10.1039/d2tc01258h.

16. T. Rosskopf, A. Dussaux, K. Ohashi, et al., "Investigation of Surface Magnetic Noise by Shallow Spins in Diamond," *Physical Review Letters* 112, no. 14 (2014): 147602, https://doi.org/10.1103/PhysRevLett.112.147602.

17. R. Schirhagl, K. Chang, M. Loretz, and C. L. Degen, "Nitrogen-Vacancy Centers in Diamond: Nanoscale Sensors for Physics and Biology," *Annual Review of Physical Chemistry* 65 (2014): 83–105, https://doi.org/10.1146/annurev-physchem-040513-103659.

18. S. Pezzagna, D. Rogalla, D. Wildanger, J. Meijer, and A. Zaitsev, "Creation and Nature of Optical Centres in Diamond for Single-Photon Emission—Overview and Critical Remarks," *New Journal of Physics* 13, no. 3 (2011): 035024, https://doi.org/10.1088/1367-2630/13/3/035024.

19. P. Spinicelli, A. Dréau, L. Rondin, et al., "Engineered Arrays of Nitrogen-Vacancy Color Centers in Diamond Based on Implantation of CN − Molecules through Nanoapertures," *New Journal of Physics* 13, no. 2 (2011): 025014, https://doi.org/10.1088/1367-2630/13/2/025014.

20. A. Watanabe, T. Nishikawa, H. Kato, et al., "Shallow NV Centers Augmented by Exploiting n-Type Diamond," *Carbon* 178 (2021): 294–300, https://doi.org/10.1016/j.carbon.2021.03.010.

21. H. Kawarada, "Hydrogen-Terminated Diamond Surfaces and Interfaces," *Surface Science Reports* 26, no. 7 (1996): 205–206, https://doi.org/10.1016/S0167-5729(97)80002-7.

22. A. Stacey, N. Dontschuk, J.-P. Chou, et al., "Evidence for Primal sp 2 Defects at the Diamond Surface: Candidates for Electron Trapping and Noise Sources," *Advanced Materials Interfaces* 6, no. 3 (2019): 1801449, https://doi.org/10.1002/admi.201801449.

23. M. V. Hauf, B. Grotz, B. Naydenov, et al., "Chemical Control of the Charge state of Nitrogen-Vacancy Centers in Diamond," *Physical Review B* 83, no. 8 (2011): 081304, https://doi.org/10.1103/PhysRevB.83.081304.

24. M. Mertens, M. Mohr, K. Brühne, et al., "Patterned Hydrophobic and Hydrophilic Surfaces of Ultra-Smooth Nanocrystalline Diamond Layers," *Applied Surface Science* 390 (2016): 526–530, https://doi.org/10.1016/j.apsusc.2016.08.130.

25. C. Osterkamp, J. Scharpf, S. Pezzagna, et al., "Increasing the Creation Yield of Shallow Single Defects in Diamond by Surface Plasma Treatment," *Applied Physics Letters* 103, no. 19 (2013): 193118, https://doi.org/10.1063/1.4829875.

26. K.-M. C. Fu, C. Santori, P. E. Barclay, and R. G. Beausoleil, "Conversion of Neutral Nitrogen-Vacancy Centers to Negatively Charged Nitrogen-Vacancy Centers through Selective Oxidation," *Applied Physics Letters* 96, no. 12 (2010): 121907, https://doi.org/10.1063/1.3364135.

27. G. Alba, M. P. Villar, R. Alcántara, J. Navas, and D. Araujo, "Surface States of (100) O-Terminated Diamond: Towards Other 1 × 1:O Reconstruction Models," *Nanomaterials* 10, no. 6 (2020): 1193, https://doi.org/10.3390/nano10061193.

28. J. Navas, D. Araujo, J. C. Piñero, et al., "Oxygen Termination of Homoepitaxial Diamond Surface by Ozone and Chemical Methods: An Experimental and Theoretical Perspective," *Applied Surface Science* 433 (2018): 408–418, https://doi.org/10.1016/j.apsusc.2017.10.065.

29. M. Kim, H. J. Mamin, M. H. Sherwood, C. T. Rettner, J. Frommer, and D. Rugar, "Effect of Oxygen Plasma and Thermal Oxidation on Shallow Nitrogen-Vacancy Centers in Diamond," *Applied Physics Letters* 105, no. 4 (2014): 042406, https://doi.org/10.1063/1.4891839.

30. P. E. Pehrsson and T. W. Mercer, "Oxidation of Heated Diamond C(100):H Surfaces," *Surface Science* 460 (2000): 74–90, https://doi.org/10.1016/S0039-6028(00)00495-7.

31. P. E. Pehrsson and T. W. Mercer, "Oxidation of the Hydrogenated Diamond (100) Surface," *Surface Science* 460 (2000): 49–66, https://doi.org/10.1016/S0039-6028(00)00494-5.

32. F. Klauser, S. Ghodbane, R. Boukherroub, et al., "Comparison of Different Oxidation Techniques on Single-Crystal and Nanocrystalline Diamond Surfaces," *Diamond and Related Materials* 19, no. 5-6 (2024): 474–478.

33. J. Fuhrmann, J. Lang, J. Scharpf, et al., "Probing Coherence Properties of Shallow Implanted NV Ensembles under Different Oxygen Terminations," *Materials for Quantum Technology* 4, no. 4 (2024): 041001, https://doi.org/10.1088/2633-4356/ad9376.

34. C. Findler, J. Lang, C. Osterkamp, M. Nesládek, and F. Jelezko, "Indirect Overgrowth as a Synthesis Route for Superior Diamond Nano Sensors," *Scientific Reports* 10, no. 1 (2020): 22404, https://doi.org/10.1038/s41598-020-79943-2.

35. K. J. Brown, E. Chartier, E. M. Sweet, D. A. Hopper, and L. C. Bassett, "Cleaning Diamond Surfaces Using Boiling Acid Treatment in a Standard Laboratory Chemical Hood," *Journal of Chemical Health & Safety* 26, no. 6 (2019): 40–44, https://doi.org/10.1016/j.jchas.2019.06.001.

36. T. Teraji, Y. Koide, and T. Ito, "Schottky Barrier Height and Thermal Stability of p-diamond (100) Schottky Interfaces," *Thin Solid Films* 557 (2014): 241–248, https://doi.org/10.1016/j.tsf.2013.11.132.

37. R. Ohta, N. Saito, Y. Inoue, H. Sugimura, and O. Takai, "Organosilane Self-Assembled Monolayers Directly Linked to the Diamond Surfaces," *Journal of Vacuum Science & Technology A: Vacuum, Surfaces, and Films* 22, no. 5 (2004): 2005–2009, https://doi.org/10.1116/1.1776184.

38. F. Fávaro de Oliveira, S. A. Momenzadeh, Y. Wang, et al., "Effect of Low-Damage Inductively Coupled Plasma on Shallow Nitrogen-Vacancy Centers in Diamond," *Applied Physics Letters* 107, no. 7 (2015): 73107, https://doi.org/10.1063/1.4929356.

39. S. Sangtawesin, B. L. Dwyer, S. Srinivasan, et al., "Origins of Diamond Surface Noise Probed by Correlating Single-Spin Measurements with Surface Spectroscopy," *Physical Review X* 9, no. 3 (2019): 031052, https://doi.org/10.1103/PhysRevX.9.031052.

40. F. Maier, J. Ristein, and L. Ley, "Electron Affinity of Plasma-hydrogenated and Chemically Oxidized Diamond (100) Surfaces," *Physical Review B* 64, no. 16 (2001): 165411, https://doi.org/10.1103/PhysRevB.64.165411.

41. J. Vig and J. LeBus, "UV/Ozone Cleaning of Surfaces," *IEEE Transactions on Parts, Hybrids, and Packaging* 12, no. 4 (1976): 365–370, https://doi.org/10.1109/TPHP.1976.1135156.

42. J. F. S. Da Petruci, D. N. Barreto, M. A. Dias, E. P. Felix, and A. A. Cardoso, "Analytical Methods Applied for Ozone Gas Detection: A Review," *TrAC Trends in Analytical Chemistry* 149 (2022): 116552, https://doi.org/10.1016/j.trac.2022.116552.

43. C.-C. Chiang, H.-H. Wan, J.-S. Li, F. Ren, and S. J. Pearton, "Ultra-smooth Single-Crystal Diamond Surfaces by Extended Ozone Exposure," *Journal of Vacuum Science & Technology A* 43, no. 4 (2025): 043110, https://doi.org/10.1116/6.0004590.

44. J. Ackermann and A. Krueger, "Efficient Surface Functionalization of Detonation Nanodiamond Using Ozone under Ambient Conditions," *Nanoscale* 11, no. 16 (2019): 8012–8019, https://doi.org/10.1039/c9nr01716j.

45. J. Ackermann and A. Krueger, "Highly Sensitive and Reproducible Quantification of Oxygenated Surface Groups on Carbon Nanomaterials," *Carbon* 163 (2020): 56–62, https://doi.org/10.1016/j.carbon.2020.02.088.

46. O. Shenderova, A. Koscheev, N. Zaripov, et al., "Surface Chemistry and Properties of Ozone-Purified Detonation Nanodiamonds," *The Journal of Physical Chemistry C* 115, no. 20 (2011): 9827–9837, https://doi.org/10.1021/jp1102466.

47. H. Yamano, S. Kawai, K. Kato, et al., "Charge state Stabilization of Shallow Nitrogen Vacancy Centers in Diamond by Oxygen Surface Modification," *Japanese Journal of Applied Physics* 56 (2017): 04CK08, https://doi.org/10.7567/JJAP.56.04CK08.

48. A. Fujimoto, Y. Yamada, M. Koinuma, and S. Sato, "Origins of sp 3 C peaks in C 1s X-Ray Photoelectron Spectra of Carbon Materials," *Analytical Chemistry* 88, no. 12 (2016): 6110–6114, https://doi.org/10.1021/acs.analchem.6b01327.

49. R. Graupner, F. Maier, J. Ristein, L. Ley, and C. Jung, "High-Resolution Surface-Sensitive C 1 *s* Core-Level Spectra of Clean and Hydrogen-Terminated Diamond (100) and (111) Surfaces," *Physical Review B* 57 (1998): 12397–12409, https://link.aps.org/doi/10.1103/PhysRevB.57.12397.

50. S. R. Haines, K. H. Williams, N. Almond, et al., "The Initial Stages of Graphite Formation on the Diamond (100) 2×1 Surface," *Journal of Electron Spectroscopy and Related Phenomena* 152 (2006): 33–36, https://doi.org/10.1016/j.elspec.2006.03.002.

51. M. C. Biesinger, "Accessing the Robustness of Adventitious Carbon for Charge Referencing (Correction) Purposes in XPS Analysis: Insights from a Multi-User Facility Data Review," *Applied Surface Science* 597 (2022): 153681, https://doi.org/10.1016/j.apsusc.2022.153681.

52. J. F. Barry, J. M. Schloss, E. Bauch, et al., "Sensitivity Optimization for NV-Diamond Magnetometry," *Reviews of Modern Physics* 92, no. 1 (2020): 015004, https://doi.org/10.1103/RevModPhys.92.015004.

53. P. Chrostoski, P. Kehayias, and D. H. Santamore, "Surface Roughness Noise Analysis and Comprehensive Noise Effects on Depth-dependent Coherence Time of NV Centers in Diamond," *Physical Review B* 106, no. 23 (2022): 235311, https://doi.org/10.1103/PhysRevB.106.235311.

54. W. Kulisch, C. Popov, D. Gilliland, G. Ceccone, F. Rossi, and J. P. Reithmaier, "Investigation of the UV/O 3 Treatment of Ultra-nanocrystalline Diamond Films," *Surface and Interface Analysis* 42 (2010): 1152–1155, https://doi.org/10.1002/sia.3264.

55. T. Sakai, K.-S. Song, H. Kanazawa, et al., "Ozone-Treated Channel Diamond Field-Effect Transistors," *Diamond and Related Materials* 12 (2003): 1971–1975, https://doi.org/10.1016/S0925-9635(03)00277-2.

56. R. Vidrio, D. Vincent, B. Bachman, et al., "XPS Analysis of Molecular Contamination and sp ^{2} Amorphous Carbon on Oxidized (100) Diamond," *Materials for Quantum Technology* 4, no. 2 (2024): 025201, https://doi.org/10.1088/2633-4356/ad4e8a.

57. A. M. Zaitsev, *Optical Properties of Diamond: A Data Handbook*, (Springer Nature, 2001), https://doi.org/10.1007/978-3-662-04548-0.

58. N. Aslam, G. Waldherr, P. Neumann, F. Jelezko, and J. Wrachtrup, "Photo-induced Ionization Dynamics of the Nitrogen Vacancy Defect in Diamond Investigated by Single-Shot Charge State Detection," *New Journal of Physics* 15, no. 1 (2013): 013064, https://doi.org/10.1088/1367-2630/15/1/013064.

59. T. Kageura, Y. Sasama, T. Teraji, et al., "Spin-State Control of Shallow Single NV Centers in Hydrogen-Terminated Diamond," *ACS Applied Materials & Interfaces* 16, no. 10 (2024): 13212–13218, https://doi.org/10.1021/acsami.3c17544.

60. R. Santagati, A. A. Gentile, S. Knauer, et al., "Magnetic-Field Learning Using a Single Electronic Spin in Diamond with One-Photon Readout at Room Temperature," *Physical Review X* 9, no. 2 (2019): 021019, https://doi.org/10.1103/PhysRevX.9.021019.

61. R. Fukuda, P. Balasubramanian, I. Higashimata, et al., "Lithographically Engineered Shallow Nitrogen-Vacancy Centers in Diamond for External Nuclear Spin Sensing," *New Journal of Physics* 20, no. 8 (2018): 083029, https://doi.org/10.1088/1367-2630/aad997.

62. P. L. Stanwix, L. M. Pham, J. R. Maze, et al., "Coherence of Nitrogen-vacancy Electronic Spin Ensembles in Diamond," *Physical Review B* 82, no. 20 (2010): 201201, https://doi.org/10.1103/PhysRevB.82.201201.

63. G. de Lange, Z. H. Wang, D. Ristè, V. V. Dobrovitski, and R. Hanson, "Universal Dynamical Decoupling of a Single Solid-State Spin from a Spin Bath," *Science* 330, no. 6000 (2010): 60–63, https://doi.org/10.1126/science.1192739.

64. J. F. Barry, M. H. Steinecker, S. T. Alsid, et al., "Sensitive ac and Dc Magnetometry with Nitrogen-Vacancy-Center Ensembles in Diamond," *Physical Review Applied* 22, no. 4 (2024): 044069, https://doi.org/10.1103/PhysRevApplied.22.044069.

65. S. Kono, T. Kageura, Y. Hayashi, et al., "Carbon 1s X-Ray Photoelectron Spectra of Realistic Samples of Hydrogen-Terminated and Oxygen-Terminated CVD Diamond (111) and (001)," *Diamond and Related Materials* 93 (2019): 105–130, https://doi.org/10.1016/j.diamond.2019.01.017.

66. P. J. Cumpson and M. P. Seah, "Elastic Scattering Corrections in AES and XPS. II. Estimating Attenuation Lengths and Conditions Required for Their Valid Use in Overlayer/Substrate Experiments," *Surface and Interface Analysis* 25, no. 6 (1997): 430–446, https://doi.org/10.1002/(SICI)1096-9918(199706)25.

Supporting Information

Additional supporting information can be found online in the Supporting Information section.

Supporting File: qute70288-sup-0001-SuppMat.docx.